ADVANCED FUNCTIONAL MATERIALS
www.afm-journal.de

Stretchable Chemical Patterns for the Assembly and Manipulation of Arrays of Microdroplets with Lensing and Micromixing Functionality

*John J. Bowen, Jay M. Taylor, Christopher P. Jurich, and Stephen A. Morin**

The chemical properties of a surface are readily controlled using a layer (or layers) of surface-functional groups that can be generated with, for example, self-assembled monolayers (SAMs) or polymer brushes. These methods have enabled rational control over surface chemistry, which directly impacts surface properties, such as wettability, but generally follow a serial approach to building up surface-functional groups (i.e., separate chemical steps are needed for the initial and each subsequent surface modification). This paper describes systems based on soft materials—stretchable chemical patterns—that have surface properties that are easily and reversibly modified using mechanical deformations. These systems couple surface-chemical features such as the density and arrangement of functional groups on elastomeric polymers (e.g., polydimethylsiloxane) to mechanically induced surface deformations. This approach enables rapid and reversible control of surface chemistry and thus surface properties and processes. The behavior of these systems is characterized using fluorescent molecules and their utility illustrated through the organization and manipulation of arrays of micrometer-scale droplets, which have optical and small-volume mixing functionalities applicable to microlens and microreactor technologies, respectively. The capabilities of these systems may be extended to, for example, the control of heterogeneous nucleation, surface reactivity, and micro/nanoscale assembly.

1. Introduction

Established methods for building precise surface-chemical patterns (e.g., the deposition of alkanethiols on gold films to form self-assembled monolayers, SAMs[1]) are suited for the fabrication of predetermined arrays of functional groups on rigid, planar substrates. These approaches work best with (or experimentally require) substrates made of hard materials. Modifications to the surface-chemical features generated following these techniques are generally constrained to additional processing steps, which may be difficult, slow, or irreversible. The surface-chemical features (e.g., the pattern, density, and orientation of surface functional groups) of these rigid materials are therefore difficult to modify rapidly and reversibly. We desire simple systems with surface-chemical features that can be easily and reversibly modified using mechanical stimuli. The tunable surface properties of these systems will be useful, for example, in controlling surface wettability, reactivity, and assembly.

We describe an approach where the surfaces of soft, elastomeric polymers are covalently functionalized with desired chemical moieties that are reversibly modified using mechanical deformations. We demonstrate this approach using soft materials with micrometer-scale patterns of chemical functional groups on their surface. Specifically, we homogeneously and heterogeneously functionalized silicone films with small molecules and fluorophores and demonstrated rational control of critical surface-chemical features (e.g., pattern, area, and molecular density) of these films using stress-induced strain. We applied tensile stress to the films after or during the process of functionalization to decrease or increase (following the release of the stress), respectively, the feature size and periodicity of the chemical patterns on the films. Further, when we applied tensile stress to the polymers during functionalization, we were able to access an array of patterns from one mask design by controlling the axis of stress. This approach will enable functional materials with surface properties (e.g., surface energy) and features (e.g., the size and/or organization of reactive/inert and/or wettable, to select solvents, regions) that can be controlled using mechanical deformation. Finally, we used the chemical and mechanical functionality of these materials to organize and manipulate the geometry of arrays of liquid droplets on their surfaces by stretching the films. These arrays of microdroplets have functionality applicable to microlens and microreactor technologies, and again, by stretching the elastomeric supports, it is possible to tune the geometric properties (and thus function) of the droplet arrays.

One of the most common and versatile methods available for chemically functionalizing a surface is to cover it with a layer of self-organizing molecules—self-assembled monolayers (SAMs).[1] SAMs may be used to produce surfaces

J. J. Bowen, J. M. Taylor, C. P. Jurich, Prof. S. A. Morin
Department of Chemistry
University of Nebraska – Lincoln
Lincoln, NE 68588, USA
E-mail: smorin2@unl.edu
Prof. S. A. Morin
Nebraska Center for Materials and Nanoscience
University of Nebraska – Lincoln
Lincoln, NE 68588, USA

DOI: 10.1002/adfm.201502174

with well-defined homogeneous or heterogeneous arrangements of chemical functionality and are typically formed by depositing alkanethiols on thin films of precious metals (e.g., gold,[2] silver,[3] and palladium[4]). The large variety of commercially available alkanethiols with different terminal functional groups, the experimental simplicity, and the mild conditions required for the formation of SAMs have made them ubiquitous throughout the surface sciences. When combined with microcontact printing techniques, SAMs can be used to fabricate micrometer-scale patterns of chemical functionality.[5] Some of the limitations of SAMs arise from their: (i) requirement for surfaces coated in metallic thin films; (ii) need for additional processing steps to modify SAMs once they have been assembled; (iii) sensitivity to changes in surface topography during formation; and (iv) constraint that rigid support substrates be used.[1] The latter is particularly relevant to the work we describe in this paper.

In contrast to SAMs coated onto metal films, functionalization of the surface of a polymer typically involves the covalent attachment of a desired functional molecule. Polymer grafting, for example, is a method where low molecular weight polymer chains are covalently attached to a polymer surface (grafting-onto[6]) or polymerized directly on a polymer surface (grafting-from[6c,7]). The attached polymer chains, referred to as "polymer brushes," are used to control the properties of the host surface.[8] Polymer brushes can be patterned to provide well-defined surface chemistries using both top-down (through lithography[9]) and bottom-up (through self-assembly[10]) techniques. When patterned polymer brushes are combined with block copolymers (BCPs)—materials that self-assemble into 3D structures that depend on the lengths and chemistries of the copolymer chains[11]—it is possible to access nanoscale chemical patterns.[12] In this process so-called "neutral" polymer brushes direct the BCPs into the oriented nanostructures/patterns.[12] Similarly, commodity polymers (e.g., polycarbonates and polyethylene terephthalates) can be modified through UV photooxidation (homogenously or through a photomask) followed by covalent attachment of desired surface moieties.[13] The surfaces of commodity polymers can also be derivatized using photolithography.[14] As with SAMs, these systems require additional steps to modify their surface chemistries.

Elastomeric polymers (e.g., silicones, polyurethanes, and polyisoprenes) have low Young's moduli and linear stress–strain curves to large strain values.[15] The virtually exclusive use of polydimethylsiloxane (PDMS) in soft lithography and microfluidics has yielded a number of chemical functionalization strategies that generally begin with oxidation to yield hydroxyl moieties.[16] These hydroxyl groups are subsequently modified via reaction with silanes such as 3-aminopropyltriethoxysilane (APTES) (Figure S1, Supporting Information).[17] This approach is versatile and has been used to attach DNA to PDMS substrates,[17c,d] to functionalize PDMS films with biomolecules,[17f] and to impart PDMS structures with resistance to nonspecific molecular adsorption.[17e] There are also examples where alkyltrichlorosilanes are used to create monolayers on the surface of disordered polymers such as PDMS, and these demonstrations show that the properties of the monolayers can approach those achievable using rigid substrates (e.g., gold and silicon).[18] When the mechanical properties of PDMS are coupled with surface modification, either through coatings or chemical modification, it is also possible to modify surface topography, through controlled wrinkling/buckling, as well as surface chemistry.[19]

2. Experimental Design

We chose to use PDMS because: (i) the mechanical properties of PDMS are well established,[15,20] (ii) the chemical modification of PDMS is straightforward and numerous methods exist (e.g., oxidation followed by derivitization[17b–f] and UV-initiated polymer grafting[21,17a,22]) and (iii) the transparency of PDMS in the visible spectrum makes observation using optical methods convenient and is useful for many optical applications. The approach we describe is, however, not limited to PDMS—other silicone and nonsilicone based elastomers (e.g., thermoplastic urethanes or natural rubbers) may also be used. The elongation at breakage (160%) and Young's modulus (reported to range from 1.32 to 2.97 MPa,[20,23] and experimentally measured at 1.32 MPa in this study, Figure S2, Supporting Information) of PDMS are ideal for investigating a range of strain states at reasonable magnitudes of stress convenient for benchtop experiments (6.5 N of tensile force is required to achieve a strain of 3.2 when thin, 0.5 mm × 7.5 mm, films are used). The elastic region of the stress–strain curve of PDMS (Figure S2, Supporting Information) extends to strains of ≈3 and insured that large strains were possible without plastic deformation of the material.

We functionalized PDMS by oxidizing the surface and then covalently attached (through the resulting silanol groups) primary amines (**Figure 1**A–D, and Figures S1 and S3 in the Supporting Information), which are easily derivatized following several approaches (Figure S1, Supporting Information).[17] For example, primary amines react directly with isothiocyanates and carboxylic acids (using 1-ethyl-3-(3-dimethylaminopropyl) carbodiimide (EDC)/N-hydroxysuccinimide (NHS) coupling for the latter[22]) providing pathways to numerous terminal functional groups in a single step. Primary amines may also be coupled to sulfo-(*N*-maleimidomethyl) cyclohexane-1-carboxylate (sulfo-SMCC)[24] or bis(sulfosuccinimidyl) suberate (BS3),[17f] which provide thiol or amine-reactive terminal groups, respectively. The diversity of this chemistry provides easy access to the vast range of functional groups represented in commercially available compounds. These approaches use benign reaction conditions (i.e., aqueous solutions at/near room temperature and close to neutral pH) that are compatible with many materials, including elastomeric polymers such as PDMS.

We covalently attached fluorescent molecules to the amine-patterned PDMS films (Figure 1A–D) to enable the use of fluorescence microscopy to visualize micrometer-scale, stress-induced changes to the functionalized surface directly. We chose to use fluorescence over other methods because: (i) the relatively high signal to noise ratio of fluorescence-based images provides better contrast than optical images of visible wavelength dye molecules, (ii) the chemistry used in the linkage of fluorescent probes is compatible with amine-functionalized surfaces as well as others (e.g., thiol or carboxylic acid terminated surfaces), and (iii) the transparency of

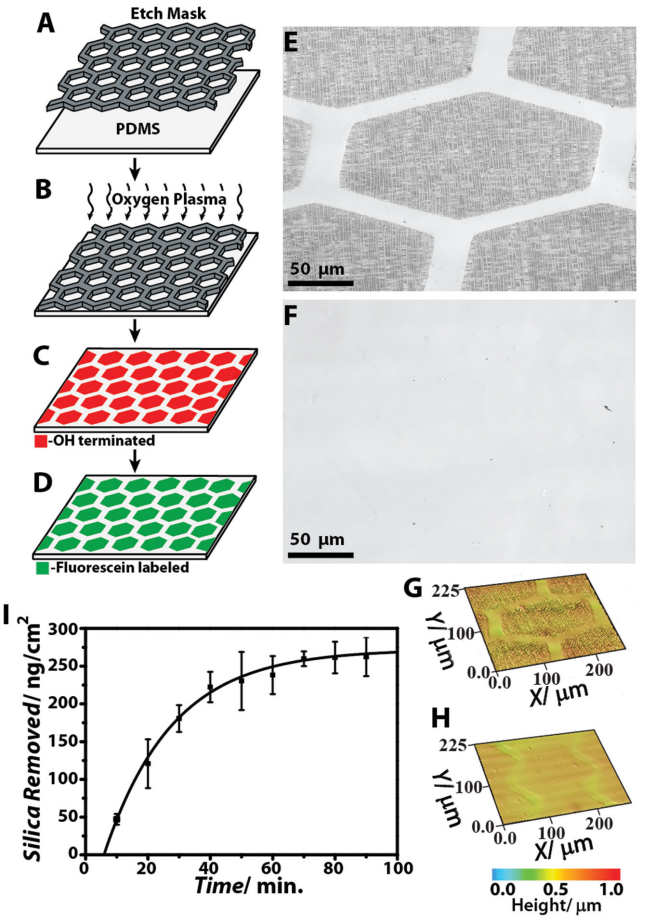

Figure 1. Schematic illustrating the functionalization process. A) An etch mask was pressed onto a PDMS film. B) The polymer film was exposed to oxygen plasma. C) Patterned, hydroxyl-terminated regions result. D) The film was reacted with APTES and FITC in a phosphate buffered pH 7 solution yielding an array of fluorescently labeled regions. E,F) Confocal micrographs of stretched PDMS films: E) film imaged directly following oxidation and F) film that was oxidized and soaked in phosphate buffered pH 7 solution at 80 °C for 1 h. G,H) Contour maps of the stretched PDMS films in panels (E) and (F), respectively, generated from optical sections collected using confocal microscopy: G) the oxidized film and H) the oxidized/buffer soaked film (the maps share the same height scale). I) Silica dissolution from an oxidized PDMS film as a function of time (films were soaked in a 0.1 M NaCl solution).

many fluorescent molecules to visible light enables the use of standard optical imaging for structural analysis without interference from absorption. Furthermore, we can use fluorescence intensity as a function of strain to estimate changes in surface-molecular density and to monitor changes to the area of the patterned regions.

We generated polygonal arrays of chemically distinct regions on the surface of the films because deformations of these shapes were easily measured by observing changes to the standard angles and side lengths of the polygons. These observations provided convenient data sets for quantifying the magnitude(s) and axis (axes) of strain, ε, defined by Equation (1):

$$\varepsilon = (\Delta L + L)/L \quad (1)$$

where ΔL and L are the change in length and initial length of the film, respectively (**Figure 2**A,B and Figure S4, Supporting Information). We could have also used patterns consisting of shapes with curves, such as circles or ellipses, and the shapes need not be symmetric.

We chose to stretch the polymer because tensile stress is an experimentally convenient method to access a large range of deformations. Compression can access different strain states as well but can induce surface deformations (i.e., rippling), which would be problematic for analysis using optical microscopy. We stretched the elastomeric films using home-built tensioning devices (Figure S5 and Video S1, Supporting Information) because it was critical that these devices interface directly with

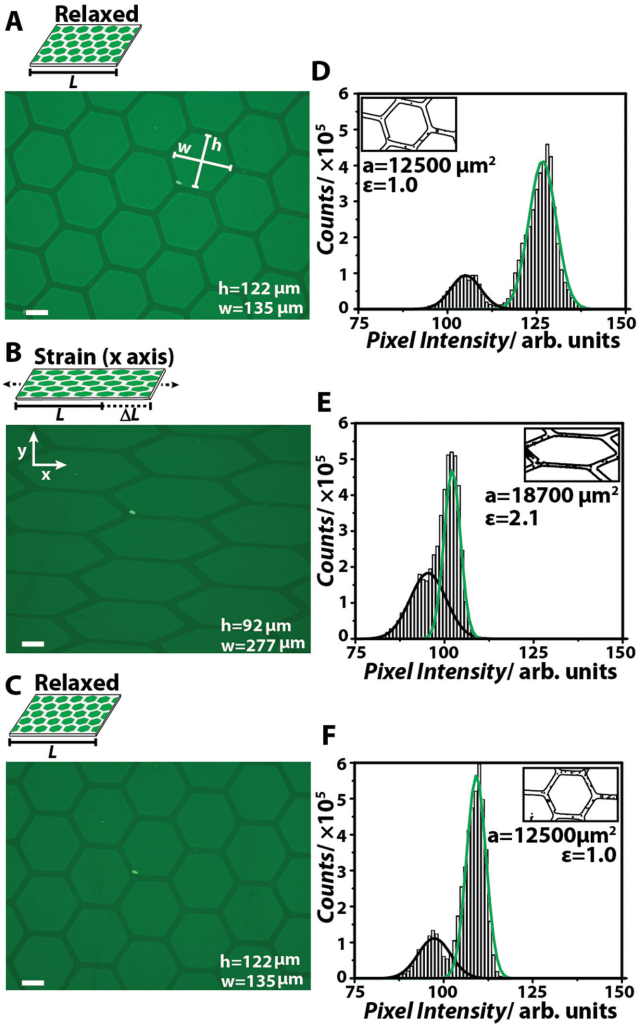

Figure 2. Uniaxial stress cycle of a heterogeneously functionalized PDMS film. A) Fluorescence micrograph of the film in a relaxed state ($\varepsilon = 0$). B) The film was stressed to a strain of $\varepsilon = 2.1$ along the *x*-axis (axes are indicated by annotation). C) The film was returned to a relaxed state ($\varepsilon = 0$). Inset are the height (h) and width (w) of the hexagons as defined in panel (A). D–F) Pixel intensity histograms of the green channel of the corresponding micrographs in the left column. The green Gaussian curve corresponds to the hexagonal area functionalized with FITC, while the black curve corresponds to the unfunctionalized native PDMS. Inset are traces of the pattern used to calculate the area (a) of the hexagons, the state of strain (ε), and the surface Poisson's ratio. All scale bars are 50 μm.

a standard (horizontal optical axis) microscope. The geometries of commercial material testing devices (e.g., the Instron system used in stress–strain measurements, see the Supporting Information) are not easily integrated with a horizontal axis microscope. Furthermore, for observing a constant position on the polymer surface throughout an experiment, it was critical to pull equally from both ends—a mode of operation not used by most commercial instruments. We used both static (based on tensioning screws) and electromechanical devices (Figure S5, Supporting Information).

3. Results and Discussion

3.1. Chemical Functionalization

We used oxygen plasma activation as the first step of functionalization as is typical for the derivitization of PDMS;[17a,17c–f] however, the treatment of PDMS with oxygen plasma is accompanied by the formation of a layer of brittle silica on the polymer surface that will crack and wrinkle when the polymer is stretched.[16] Here we employed two strategies to avoid the undesired mechanical effects of a silica layer, thus maintaining the elasticity of the PDMS surface: (i) we minimized both the time that the polymer is exposed to plasma and the power of the oxygen plasma and (ii) we removed (via chemical dissolution) the thin silica layer formed on the oxidized PDMS *prior* to stressing the polymer. The latter was critically important as we always observed crack formation on the surface of the PDMS films when they were stretched (or otherwise deformed) prior to removal of the silica layer (Figure 1E–H and Figures S6–S9, Supporting Information). This strategy benefits from the morphology of the silica—a thin, porous layer on the PDMS surface[16]—and the ability of relatively benign solutions (e.g., common buffers and briny solutions) to slowly etch silica.[25]

Silanol groups remained on the PDMS films through silica dissolution and it was to these groups that we attached amine-terminated alkanes (Figure 1A–D and Figure S1, Supporting Information). We then covalently attached fluorescein isothiocyanate (FITC) to these aminated regions for visualization of the chemical patterns using fluorescence microscopy (Figure 2A and Figure S4, Supporting Information). We monitored the surface-chemical changes associated with each step of derivitization by measuring the contact angle of water (Table S1, Supporting Information). As expected based on previous studies,[16] hydroxyl moieties are unstable in air prior to derivitization. We therefore minimized the time oxidized PDMS films were exposed to air between oxidation and functionalization. Once derivatized with amine groups and FITC, the surfaces of the PDMS films were relatively stable in air up to at least 120 min. If the samples were stored in buffer solution (100×10^{-3} M, pH 7, see the Supporting Information), the surfaces were stable for many hours (Table S1, Supporting Information).

3.2. Uniaxial Stress

We subjected the films to stress cycles while visualizing the changes to the patterns using fluorescence microscopy (Figure 2A–C and Video S2, Supporting Information). The ability to visualize the dynamic changes to micrometer-scale chemical patterns directly during mechanical deformation provides information that compliments the surface-structural information obtained from confocal and atomic force microscopy studies (Figure 1E–H, and Figures S6 and S7, Supporting Information) and surface-chemical information from contact angle measurements (Table S2, Supporting Information). For example, changes to the intensity histograms at different states of strain indicated changes in the density of the surface-bound chemical moieties (FITC in this case, but by extension we expect the same to hold for other functional groups). We used these shifts in the intensity distribution with stress as a semiquantitative indicator of the changes to the number of fluorescent molecules per unit area. We observed a loss in total fluorescence during these studies that we attribute to photobleaching of the fluorophore and not mechanical cycling—the fluorescent patterns were stable through many cycles of stress but weakened in intensity when imaged repeatedly due to the increased exposure to light (Figure S10, Supporting Information). Based upon the observed shifts of the intensity peaks we estimated a change in molecular density of 16% for a uniaxial strain of $\varepsilon = 2$ (Figure 2D–F; see the Supporting Information for details on the image analysis performed). In this estimate we assume the starting density of APTES to be 9×10^{-24} mol nm^{-2} and therefore,[26] if we assume full coverage of FITC, a percent change of 16% in density would correspond to a decreased molecular density of 7×10^{-24} mol nm^{-2}. We note that throughout the stress cycle the surface microstructure of the film remained constant (Figure 2; and Video S2 and Figure S4, Supporting Information). If a brittle silica layer was intentionally left in place, cracking was also apparent in the fluorescent images (Figure S11, Supporting Information)—something we did not observe under the standard conditions used in these studies.

The Poisson's ratio of a material describes how strain along the transverse axis changes relative to axial strain. In PDMS, the Poisson's ratio is roughly 0.5.[20,23b] We used the observed changes to the area and geometry of the surface-chemical patterns as the film is stressed to calculate the surface Poisson's ratio of the functionalized PDMS films. In our experiments the surface Poisson's ratio calculated from these changes was ≈0.8, which is close to the bulk value.[20,23b] We believe this close agreement with bulk PDMS further indicates an elastic surface, free of a silica layer. The Poisson's ratio of PDMS insured that when the films were stressed uniaxially the area of the polygons that make up the chemical patterns would increase. In this case, at a strain of 2.1 the area increased by roughly 50% (Figure 2E). When stress was released the original area was recovered without evidence of plastic deformation (Figure 2F).

We further measured the changes in the surface chemistry over multiple stress cycles by monitoring contact angles (Table S2, Supporting Information). In general, whether stored in air or buffered solution, amine and FITC-terminated PDMS films were more stable through cycles of strain than hydroxylated films. We believe this observation could be due to the bulk of the amine-terminated alkyl chains and FITC molecules. As the modified films were stretched, native PDMS polymer chains were exposed at the surface, making the surface more hydrophobic, as evidenced by an increase in contact angle (Table S3,

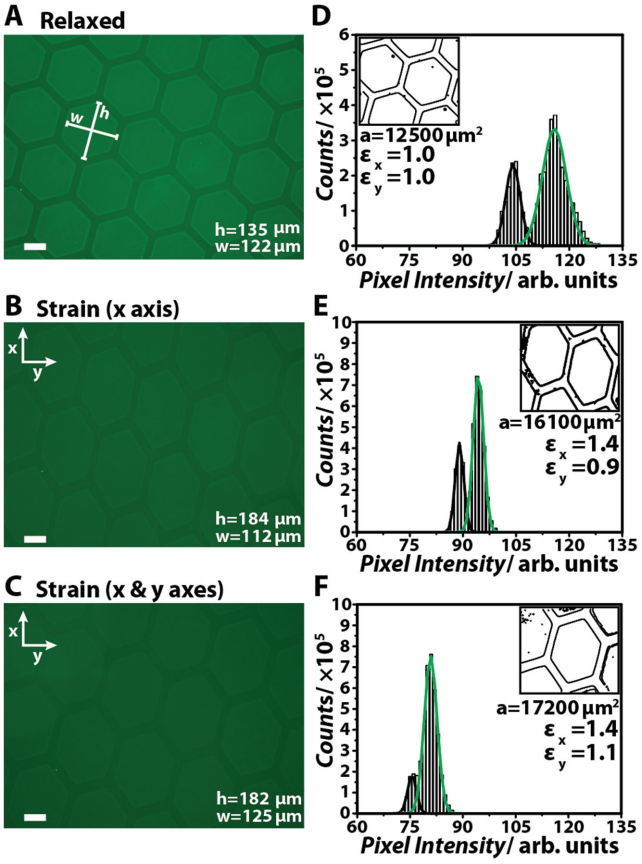

Figure 3. Biaxial stress cycle of a heterogeneously functionalized PDMS film. A) Fluorescence micrograph of film in the relaxed state ($\varepsilon = 0$). Inset are the characterisitc width (w) and height (h) of the hexagons. B) The film was held along the y-axis and stressed to a strain of $\varepsilon_x = 1.4$ along the x-axis (axes are indicated by annotation). C) The film was held along the x-axis and stressed along the y-axis to a strain of $\varepsilon_y = 1.1$ (axes are indicated by annotation). D–F) Pixel intensity histograms of the green channel of the corresponding micrograph in the left column. The green Gaussian curve corresponds to the hexagonal area functionalized with FITC, while the black curve corresponds to the unfunctionalized native PDMS. Inset are traces of the pattern used to calculate the area (a) of the hexagons and the state of strain along x and y (ε_x and ε_y, respectively). All scale bars are 50 μm.

Supporting Information). These surfaces are also mechanically stable through multiple cyles of stress (Figure S12, Supporting Information).

3.3. Biaxial Stress

We examined changes to the surface-chemical patterns on the PDMS films when stressed along two orthogonal axes. This approach allows access to 2D geometric patterns that increase in or maintain the characteristic lengths in multiple directions within the 2D plane of the surface (the surface-volume conservation required by the Poisson effect is satisfied by a corresponding decrease in film thickness). Here we demonstrated this concept by increasing the length of a film along one axis while holding and slightly increasing its length along the other (**Figure 3**A–C). When $\varepsilon_x = 1.4$ and $\varepsilon_y = 1.1$, the area of a single hexagon was increased by 38%. The corresponding intensity shifts indicated that molecular density decreased by ≈30% (Figure 3D–F). This decrease in density is roughly a factor of two larger than the uniaxial experiments, enabling access to a greater range of molecular densities. It seemed counterintuitive that a smaller percentage increase in area would translate to a larger decrease in molecular density relative to the density change observed in the uniaxial experiments. We attribute this observation to the simultaneous decrease in density along the strain axis and increase in density orthogonal to this axis (dictated by the contraction described by Poisson's ratio) that occurs in uniaxial deformation. This process is unlike the biaxial experiments where surface density must decrease along both axes of stress.

3.4. Functionalization of Stretched Films

By applying uniaxial stress to the PDMS films ($\varepsilon \approx 2$) during the chemical functionalization (**Figure 4**A–D), we were able to shrink (along one axis) the feature size of the chemical patterns relative to those of the etch mask and increase the molecular density on the surface (Figure 4E,F). In this demonstration an increase in molecular density of ≈24% (with a corresponding decrease in area of 28%) was achieved (Figure 4G,H). A feature observed in these patterns (Figure 4E,F) and others (Figure S13, Supporting Information) is a region at the border of each hexagon that is brighter than the interior. This anomalous feature is clearly seen as a shoulder on the majority peak in the intensity histograms (Figure 4G,H). We attribute these features to the metallic etch masks which have a "lip" along their edges that increases oxidation in these regions (Figure S13, Supporting Information).

By rotating the mask relative to the axis (or axes) of stress, we accessed an array of related patterns from a single master (Figure 4I–L). This approach made possible the fabrication of many rest-state patterns (of similar geometries but unique angles and periodicities) from a single etch mask. This capability illustrates a processing advantage unique to surface-chemical patterns synthesized on soft materials.

3.5. Mechanically Driven Assembly and Manipulation of Microscale Droplets

To demonstrate the mechanoresponsive properties of these materials, we drove the facile assembly of arrays of microdroplets on their surfaces using the geometric/chemical changes associated with mechanical deformations. Once assembled, we were able to readily manipulate the geometries of these arrays. We defined a square array of hydroxyl-rich regions on a PDMS surface and deposited droplets of ethylene glycol while the film was stressed (to $\varepsilon = 2.2$) (**Figure 5**A). These droplets were deposited (virtually) at random on the surface using a pneumatic nebulizer. As the stress on the film was released, the droplets organized onto the lower energy, polar regions (Figure 5A,B and Video S3, Supporting Information). We then stressed the film supporting the droplet array, manipulating the shape and organization of the droplets (Figure 5C and Video S3, Supporting Information). The transition from disordered to

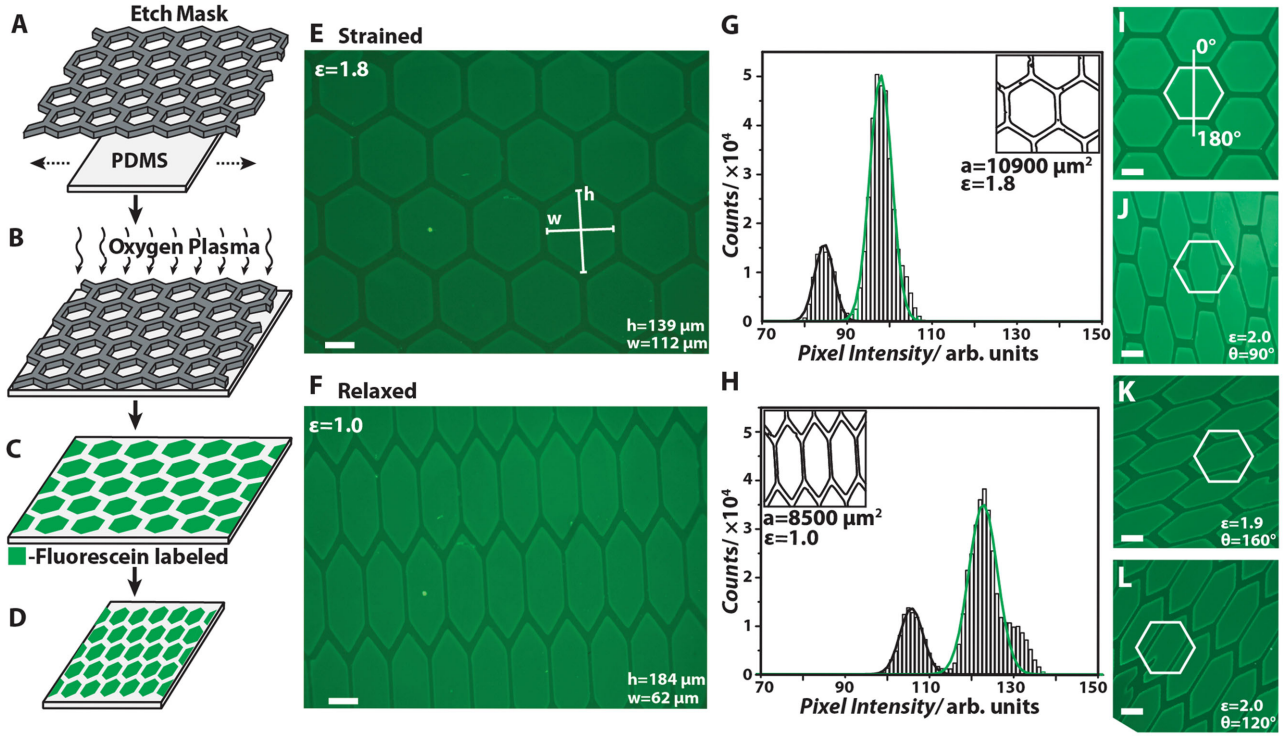

Figure 4. Functionalization of a stressed PDMS films. Schematic illustrating functionalization: A) The film was stretched and covered by an etch mask, B) exposed to oxygen plasma, and C) reacted with APTES and FITC in a phosphate buffered pH 7 solution. D) Finally, the film was relaxed. E) Fluorescence micrograph of the stretched film at strain $\varepsilon = 1.8$ corresponding to the state illustrated in panel (C), and F) relaxed corresponding to the state illustrated in panel (D). G,H) Pixel intensity histograms of the green channel of each micrograph in the left column. The green Gaussian curve corresponds to the hexagonal area functionalized with FITC, while the black curve corresponds to the unfunctionalized native PDMS. I–L) The etch mask orientation was held constant, as indicated by the solid white hexagon in each panel, during oxygen plasma treatment, and the angle (θ) of the axis of stress relative to the vertical white line in panel (I) was varied from 0° to 160°. Panel (I) is a representative image before stress was released. J–L) Images of the patterns after stress was released. Inset in Panels (J)–(L) is the magnitude of strain during oxidation and the angle (θ) of the strain axis. All scale bars are 50 μm.

ordered microdroplet arrays was clearly verified using fast Fourier transform (FFT) and particle analysis techniques (Figure 5D–I and see the Supporting Information), which made possible the determination of the distribution in droplet size and the periodicity of the droplet arrays.

We observed a decrease in the number of small, randomly sized droplets as stress is released and the small droplets coalesced into larger droplets on the polar regions. This change was accompanied by the emergence of a relatively monodispersed droplet population at 4500 ± 200 μm^2 (Figure 5H, where this area is the 2D projection of the droplets onto the film surface). We estimated the volume of the droplets to be 46 ± 7 pL using confocal microscopy (Figure 5J,K and see the Supporting Information). As the droplets ordered they converged on a symmetric array (as evidenced by the periodicity in the FFTs), which, upon the reapplication of stress, became asymmetric as droplets along the *y*-axis moved closer together and droplets along the *x*-axis moved further apart (Figure 5E,F). In this demonstration, periodicity along the *x*-axis was increased by 86 μm and periodicity along the *y*-axis was decreased by 21 μm. We applied stress orthogonally to the *y*-axis (parallel to the *x*-axis), and so a square lattice was maintained (as indicated by an angle of 90° between the *x*- and *y*-axes) (Figure 5A–C). If stress was applied along a different direction this result would have changed accordingly. The as-deposited droplets did possess a degree of ordering which reflected favorable interactions between the liquid and the polar regions of the surface-chemical patterns (Figure 5A,D,G); relieving the stress on the film drove out imperfections and yielded ordered assemblies of droplets (Figure 5B,E,H). When the starting state was less ordered, as can be achieved using vapor-phase deposition, ordered arrays could still be produced (Video S4 and Figure S14, Supporting Information).

The application of specific magnitudes of stress along desired angles makes possible the rational control of droplet density, organization, and geometry. Using this functionality, we controlled the surface area of the droplet–air interface and thus processes dependent on this area, for example, the rate of evaporation from the droplets (**Figure 6**A,B). In this demonstration, the droplets of larger surface area (Figure 6B) completely evaporated after 4 h while the lower surface area dropletes remained (Figure 6A). Further, by repeatedly cycling the support substrate between stretched and relaxed states, we were able to drive mixing within the droplets. To illustrate this shear-induced mixing process we subjected an array of microdroplets to 6300 stress cycles ($\varepsilon = 2$) over a period of 35 min at which time none of the droplets remained (Figure 6C). Compared to the stretched droplet array (Figure 6B) this evaporation occurred ten times faster. We attribute this rate increase to the

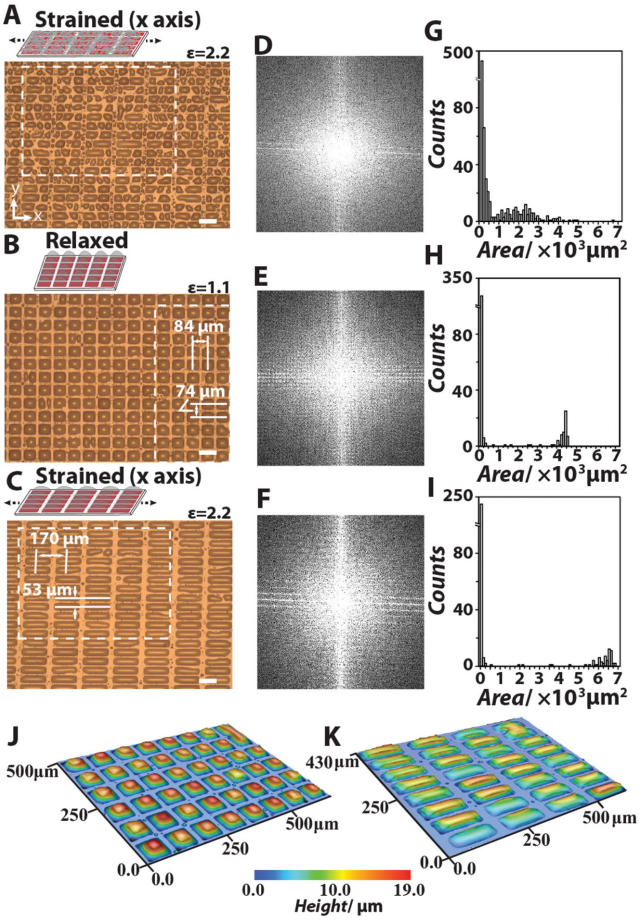

Figure 5. Driven assembly and manipulation of microdroplets. A) Droplets of ethylene glycol (80 wt% in water with 0.15 mg mL^{-1} crystal violet) were randomly deposited (using a pneumatic nebulizer) onto a stretched film that was heterogeneously patterned with polar groups. Stress was applied along the *x*-axis (axes are indicated by annotation). B) The stress on the film was released driving the assembly of the droplets into an ordered array that matched the chemical pattern. C) The periodicity of the droplet array changed by stretching the underlying film. Stress was again applied along the *x*-axis. Panels (A)–(C) have 100 μm scale bars. D–F) Fourier analysis of the area noted by the white boxes in the corresponding droplet images showing the transition from: D) a quasirandom state, to E) an ordered, square array of microdroplets, and F) the change in droplet geometry/periodicity associated with stretching the film. Analysis was performed on the same droplets and the calculated periodicities are displayed as annotations in panels (B) and (C). G–I) Analysis of the top-down area of the microdroplets shows a clear transition from: G) a broad distribution of small-area droplets, to H) a relatively monodispersed population, which I) shifts to the right as area is increased by applying stress to the film. J) Contour maps generated from optical sections collected using confocal microscopy of an array of microdroplets on a relaxed film and K) the same array after the film was stretched (the maps share the same height scale).

effect of mixing, which increases the rate of exchange of molecules between the interior of the droplet and its surface.

3.6. Microlensing from Liquid Microdroplets

We believe the ability to generate (potentially) larger-area arrays of microdroplets, of virtually any liquid (or solution), that are

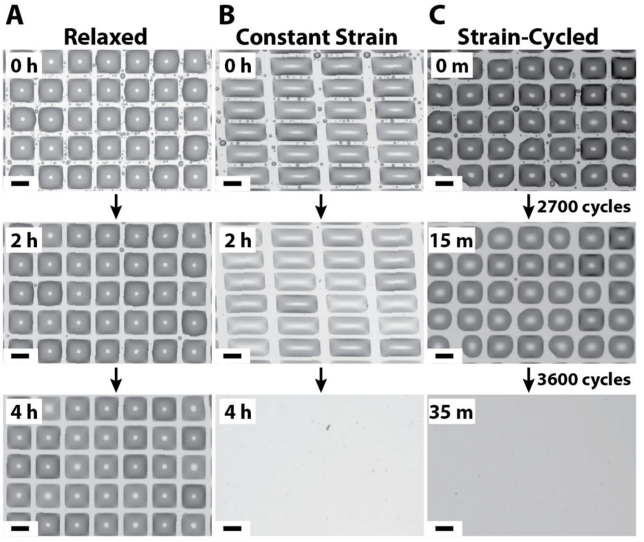

Figure 6. Controlled evaporation from microdroplets through modulation of surface area and shear-induced mixing. A) Arrays of ethylene glycol microdroplets are supported on a relaxed film, or B) stretched film (constant uniaxial strain of $\varepsilon = 1.7$) and stored in ambient conditions. Micrographs of the microdroplet arrays were collected at 0 h (top row), 2 h (middle row), and 4 h (bottom row). The same regions of the array were imaged and no droplets remained on the stretched film after 4 h (all remained on the relaxed film). C) Micrographs of a microdroplet array collected after 0 min and no stress cycles (top), after 15 min and 2700 stress cycles (middle), and 35 min and an additional 3600 stress cycles (bottom). Uniaxial strain of $\varepsilon = 2$ was applied for each stress cycle. All scale bars are 50 μm.

readily tuned using simple mechanical deformations will be useful for a number of applications. Here we focused on the optical properties of the microdroplets, which possess microlensing capabilities.[27] First, we drove the assembly of liquid (ethylene glycol was chosen for its temperature stability) microdroplets into square arrays. We then tested the optical activity of the resulting microlens arrays by observing the interference patterns generated when a collimated light source was passed through the array (**Figure 7**A,B) and by collecting images projected by the array (Figure 7C–F). For experiments with the collimated source, we directed a laser beam along the surface normal of the array and observed scattering on a screen (which was parallel to the plane of the array at a distance of 1.2 m from the film). In this case, we observed interference patterns indicative of an ordered array (a symmetric, square array) of microlenses (Figure 7B). This result was consistent with that expected for collimated light and an array of convergent lenses of small focal lengths. When we applied tensile stress to the supporting film, the observed interference patterns changed according to the increase in the axial periodicity of the array and the decrease in the transverse periodicity of the array (Figure 7B). These changes were reversible, and, because of the rapid response of the liquid lenses, easily switched between states (Video S5, Supporting Information). In our studies we were limited by the rate of extension possible using our testing systems; more rapid response should be possible with faster actuators.

We then tested the imaging properties of the array by placing an illuminated, millimeter-scale object (the letter "N") below

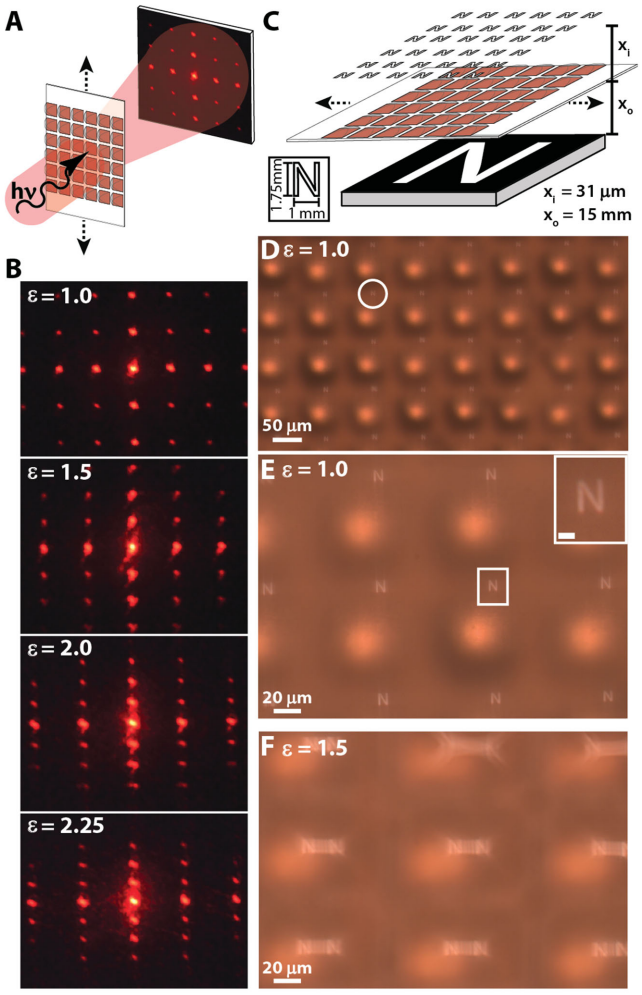

Figure 7. Liquid microlens arrays from assembled microdroplets. A) Schematic illustration of the setup used for observing the interference behavior of the microlens array: The film was stressed along the axis indicated by the dashed black arrows while a red laser ($\lambda = 650$ nm) was directed along the surface normal of the film at the center of the array and the resulting interference pattern collected on a screen 1.2 m from the film. B) The interference pattern collected at increasing strain ($\varepsilon =$ 1.0–2.25). C) Schematic illustration of the setup used to generate images with the arrays: An "N" (dimensions inset) was projected onto the microlens array (object distance, $x_o = 15$ mm) and micrographs were collected from the image plane (image distance, $x_i = 31$ μm for the unstrained film), and stress applied along the axis indicated by the black arrows. D) Low magnification micrograph of the images (one is denoted by a white circle) formed by the microlens array ($\varepsilon = 1.0$) and E) higher magnification micrograph ($\varepsilon = 1.0$). The inset of panel (E) shows an image created from a single microlens noted by the white box (inset scale bar is 4 μm). F) Split images formed when the film was stressed to a strain of $\varepsilon = 1.5$.

the array, and observing the images projected by the microlenses (Figure 7D,E). We observed lensing behavior across the array with surprisingly good uniformity considering the method of fabrication (Figure 7D). Based on the positions of the object and the images formed, we estimated the focal length of the (undeformed) lenses to be 31 μm (with deviations below the 1 μm resolution of the stage used) and the magnification to be 0.002. When the microlens array was deformed using tensile stress ($\varepsilon = 1.5$), we observed a split in the images as the droplets were pulled apart (Figure 7F). This observation was accompanied by an increase in the focal length to 37 μm, consistent with an increase in the radius of curvature for the microlenses that accompanied deformation.

4. Conclusions

We have demonstrated a general approach capable of generating micrometer-scale surface-chemical patterns with features that can be controlled—"reconfigured"—using simple mechanical stimuli. This strategy relies on the mechanical properties of soft, elastomeric polymers, and enables simple methods for controlling the microscale properties (geometry, area, etc.) and molecular-scale properties (density) of chemical patterns. By coupling mechanical stress with heterogeneous chemical functionalization we produced chemical patterns with various shapes, sizes, and periodicities that depended on the axis (or axes) of stress, the magnitude of strain, and the geometric parameters of the etch mask. In contrast to a lithographic approach operating on a rigid material, where a new mask must be used for each pattern, this approach enables families of related patterns from one master and a decrease in the feature sizes of the patterns relative to the master. This decrease in feature size is accompanied by a corresponding increase in molecular density that may be reversed by reapplying stress. This process is not limited to metallic masks with micrometer-scale polygonal features or biaxial deformations—many different patterns of different scales are accessible using etch masks fabricated from numerous materials and multiaxial deformations are possible with more advanced electromechanical systems.

We demonstrated methods for the direct visualization of the reversible stress-induced changes of surface-chemical patterns. These capabilities will be useful in expanding the understanding of the chemistry of soft material surfaces under mechanical stress and could provide methods for building functional surfaces that may, for example, be used to increase or decrease the density of surface-bound analytes and reagents. We are limited (in terms of the required deformation forces and the tolerable amounts of strain) by the Young's modulus and the elongation to fracture of PDMS, but other elastomeric polymers (e.g., Ecoflex or polyisoprene) are softer and have higher elastic limits.

We applied these systems to the driven assembly and manipulation of arrays of liquid microdroplets with lensing and micromixing capabalities. This functionality was used to control the rate of evaporation—by increasing the area of the droplet–air interface and through shear-induced mixing—from the droplets, and the optical properties of the microdroplets in both imaging and interference applications, where the latter reflects the ensemble ordering of the droplets in the array. The small-volume mixing capabilities (conceptually illustrated through the evaporation studies) can find application in surface-fluidics and microreactors; the facile assembly of liquid microlens arrays with mechanically tunable properties can be applied to optical microscopy and sensing technologies.

More generally, these materials offer the ability to tune surface chemistry, and thus chemical interactions with the

surrounding environment, using mechanical stimuli. For example, these materials could potentially lead to applications where mechanical stimuli from different sources (e.g., the motions associated with using/wearing these materials) are coupled to the properties of the material's surface. Soft, stretchable chemical patterns may also be useful in controlling the selective surface nucleation of crystals and the manipulation of micro/nanoscale materials for controlling structure–property relationships in hybrid materials.

5. Experimental Section

See the Supporting Information.

Supporting Information

Supporting Information is available from the Wiley Online Library or from the author.

Acknowledgements

The authors thank the Department of Chemistry and the Nebraska Center for Materials and Nano Science (NCMN) at the University of Nebraska–Lincoln (UNL) and UNL for start-up funds. The authors thank the Nebraska University Research Council for support through a Faculty Seed Grant funded by the Layman Fund. S.A.M. thanks the NSF for support through the Nebraska EPSCoR FIRST Award program (EPS-1004094). J.J.B. thanks Derek Sekora of the Mathias Schubert Lab of the UNL Department of Electrical Engineering for assistance with contact angle measurements. The authors thank Prof. Natele Ianno from the Department of Electrical Engineering at UNL for access to the confocal microscope in the Nebraska Engineering Research Facility.

Received: May 27, 2015
Revised: July 11, 2015
Published online: August 4, 2015

[1] J. C. Love, L. A. Estroff, J. K. Kriebel, R. G. Nuzzo, G. M. Whitesides, *Chem. Rev.* **2005**, *105*, 1103.
[2] a) R. G. Nuzzo, D. L. Allara, *J. Am. Chem. Soc.* **1983**, *105*, 4481; b) G. E. Poirier, E. D. Pylant, *Science* **1996**, *272*, 1145.
[3] a) P. E. Laibinis, G. M. Whitesides, D. L. Allara, Y. T. Tao, A. N. Parikh, R. G. Nuzzo, *J. Am. Chem. Soc.* **1991**, *113*, 7152; b) L. H. Dubois, B. R. Zegarski, R. G. Nuzzo, *J. Chem. Phys.* **1993**, *98*, 678.
[4] a) A. Carvalho, M. Geissler, H. Schmid, B. Michel, E. Delamarche, *Langmuir* **2002**, *18*, 2406; b) J. C. Love, D. B. Wolfe, R. Haasch, M. L. Chabinyc, K. E. Paul, G. M. Whitesides, R. G. Nuzzo, *J. Am. Chem. Soc.* **2003**, *125*, 2597.
[5] A. Kumar, G. M. Whitesides, *Appl. Phys. Lett.* **1993**, *63*, 2002.
[6] a) W. Zhao, G. Krausch, M. H. Rafailovich, J. Sokolov, *Macromolecules* **1994**, *27*, 2933; b) R. Jordan, K. Graf, H. Riegler, K. K. Unger, *Chem. Commun.* **1996**, 1025; c) R. Jordan, A. Ulman, J. F. Kang, M. H. Rafailovich, J. Sokolov, *J. Am. Chem. Soc.* **1999**, *121*, 1016.
[7] a) O. Prucker, J. Ruhe, *Macromolecules* **1998**, *31*, 592; b) H. G. Borner, K. Beers, K. Matyjaszewski, S. S. Sheiko, M. Moller, *Macromolecules* **2001**, *34*, 4375.
[8] M. A. C. Stuart, W. T. S. Huck, J. Genzer, M. Muller, C. Ober, M. Stamm, G. B. Sukhorukov, I. Szleifer, V. V. Tsukruk, M. Urban, F. Winnik, S. Zauscher, I. Luzinov, S. Minko, *Nat. Mater.* **2010**, *9*, 101.
[9] T. Chen, I. Amin, R. Jordan, *Chem. Soc. Rev.* **2012**, *41*, 3280.
[10] J. K. Cox, A. Eisenberg, R. B. Lennox, *Curr. Opin. Colloid Interface Sci.* **1999**, *4*, 52.
[11] F. S. Bates, G. H. Fredrickson, *Annu. Rev. Phys. Chem.* **1990**, *41*, 525.
[12] M. P. Stoykovich, M. Muller, S. O. Kim, H. H. Solak, E. W. Edwards, J. J. de Pablo, P. F. Nealey, *Science* **2005**, *308*, 1442.
[13] a) R. L. McCarley, B. Vaidya, S. Y. Wei, A. F. Smith, A. B. Patel, J. Feng, M. C. Murphy, S. A. Soper, *J. Am. Chem. Soc.* **2005**, *127*, 842; b) S. A. Morin, F. F. Amos, S. Jin, *J. Am. Chem. Soc.* **2007**, *129*, 13776.
[14] Z. Nie, E. Kumacheva, *Nat. Mater.* **2008**, *7*, 277.
[15] J. C. Lotters, W. Olthuis, P. H. Veltink, P. Bergveld, *J. Micromech. Microeng.* **1997**, *7*, 145.
[16] V. Roucoules, A. Ponche, A. Geissler, F. Siffer, L. Vidal, S. Ollivier, M. F. Vallat, P. Marie, J. C. Voegel, P. Schaaf, J. Hemmerle, *Langmuir* **2007**, *23*, 13136.
[17] a) H. Makamba, J. H. Kim, K. Lim, N. Park, J. H. Hahn, *Electrophoresis* **2003**, *24*, 3607; b) J. Genzer, K. Efimenko, *Science* **2000**, *290*, 2130; c) A. A. Vaidya, M. L. Norton, *Langmuir* **2004**, *20*, 11100; d) G. A. Diaz-Quijada, D. D. M. Wayner, *Langmuir* **2004**, *20*, 9607; e) D. P. Wu, B. X. Zhao, Z. P. Dai, J. H. Qin, B. C. Lin, *Lab Chip* **2006**, *6*, 942; f) M. Huang, B. C. Galarreta, A. Artar, R. Adato, S. Aksu, H. Altug, *Nano Lett.* **2012**, *12*, 4817.
[18] a) G. S. Ferguson, M. K. Chaudhury, H. A. Biebuyck, G. M. Whitesides, *Macromolecules* **1993**, *26*, 5870; b) M. K. Chaudhury, M. J. Owen, *J. Phys. Chem.* **1993**, *97*, 5722.
[19] a) N. Bowden, S. Brittain, A. G. Evans, J. W. Hutchinson, G. M. Whitesides, *Nature* **1998**, *393*, 146; b) S. P. Lacour, D. Chan, S. Wagner, T. Li, Z. Suo, *Appl. Phys. Lett.* **2006**, *88*, 204103; c) J. Zang, S. Ryu, N. Pugno, Q. Wang, Q. Tu, M. J. Buehler, X. Zhao, *Nat. Mater.* **2013**, *12*, 321.
[20] I. D. Johnston, D. K. McCluskey, C. K. L. Tan, M. C. Tracey, *J. Micromech. Microeng.* **2014**, *24*, 7.
[21] S. W. Hu, X. Q. Ren, M. Bachman, C. E. Sims, G. P. Li, N. Allbritton, *Anal. Chem.* **2002**, *74*, 4117.
[22] J. Bacharouche, F. Badique, A. Fahs, M. V. Spanedda, A. Geissler, J.-P. Malval, M.-F. Vallat, K. Anselme, G. Francius, B. Frisch, J. Hemmerlé, P. Schaaf, V. Roucoules, *ACS Nano* **2013**, *7*, 3457.
[23] a) K. M. Choi, J. A. Rogers, *J. Am. Chem. Soc.* **2003**, *125*, 4060; b) D. Armani, C. Liu, N. Aluru, in *12th IEEE Int. Conf. Micro. Electro Mech. Syst.*, Institute of Electrical and Electronics Engineers, New York, NY, USA, **1999**, 222.
[24] T. T. Yu, M. S. Shoichet, *Biomaterials* **2005**, *26*, 1507.
[25] J. P. Icenhower, P. M. Dove, *Geochim. Cosmochim. Acta* **2000**, *64*, 4193.
[26] D. G. Kurth, T. Bein, *Langmuir* **1993**, *9*, 2965.
[27] a) L. Dong, A. K. Agarwal, D. J. Beebe, H. Jiang, *Nature* **2006**, *442*, 551; b) D. Kang, C. Pang, S. M. Kim, H. S. Cho, H. S. Um, Y. W. Choi, K. Y. Suh, *Adv. Mater.* **2012**, *24*, 1709.